JGR Biogeosciences

RESEARCH ARTICLE
10.1029/2024JG008334

The Importance of Inland Water CO_2, CH_4, and N_2O for Summertime Greenhouse Gas Exchange With the Atmosphere in Arctic Tundra Lowlands

Melanie Martyn Rosco[1], Joshua F. Dean[2], Alberto V. Borges[3], Ove H. Meisel[2], Richard van Logtestijn[4], Geert Hensgens[1], Sergei Karsanaev[5], Trofim Maximov[5], James T. Weedon[4], Rien Aerts[4], Jorien E. Vonk[1], and A. Johannes Dolman[1,6]

[1]Department of Earth Sciences, Vrije Universiteit Amsterdam, Amsterdam, the Netherlands, [2]School of Geographical Sciences, University of Bristol, Bristol, UK, [3]Chemical Oceanography Unit, University of Liège, Liège, Belgium, [4]Section Systems Ecology, Amsterdam Institute for Life and Environment, Vrije Universiteit Amsterdam, Amsterdam, the Netherlands, [5]Siberian Branch Russian Academy of Sciences, Institute for Biological Problems of the Cryolithozone, Yakutsk, Russia, [6]NIOZ Royal Netherlands Institute for Sea Research, Texel, The Netherlands

Abstract Inland waters in Arctic landscapes act as conduits of terrestrial organic material, transporting and processing organic material into the greenhouse gases (GHGs) carbon dioxide (CO_2), methane (CH_4), and nitrous oxide (N_2O), and subsequently exchanging these gases with the atmosphere. To assess the role of inland water emissions in the Arctic GHG budget, it is necessary to quantify their emissions in relation to the terrestrial sink capacity. We present measurements of dissolved CO_2, CH_4, and N_2O from lake, pond, and low-order fluvial systems across two summers (2016–2017) in the Arctic Siberian Indigirka River tundra lowlands. During May–July 2017, the region experienced large-scale flooding, of which we captured the tail end. Using remote sensing images to upscale inland water emissions to an area of approximately 18 km^2, we calculated combined carbon (C) emissions, CO_2-C, and diffusive CH_4-C under nonflood and flooded scenarios. These ranged from 7.03 ± 1.30 Mg C d^{-1} (nonflood; mean ± SD) to 9.63 ± 1.24 Mg C d^{-1} (flooded). Integrating these values into the total C landscape exchange offset the terrestrial C sink by ∼9–∼13%. When N_2O emissions were calculated as CO_2 equivalents, these emissions were negligible relative to CO_2 and CH_4. Our study shows that in the northeast Siberian Arctic tundra, summertime CO_2 and CH_4 emissions from inland waters are a potentially important component of landscape C exchange with the atmosphere, offsetting the terrestrial sink capacity, and this may be an important consideration for constraining future Arctic responses to climate warming.

Plain Language Summary In the Arctic, lakes, ponds, and rivers release greenhouse gases (GHGs) into the atmosphere as a result of biological, chemical, and physical processes. Understanding how large these emissions are is important for predicting climate change impacts. To investigate this, we measured the levels of the three most important GHGs in ponds, lakes, and streams in an area of Arctic Siberia over two summers (2016–2017). The second year of measurements coincided with a major flooding event, allowing us to learn about the system under different conditions. We combined our measurements with satellite images that allowed us to determine the total surface area of different types of water bodies and calculate an estimate of greenhouse gas emissions from the larger study area. When we compared these emissions to the amount of carbon absorbed by the plants on land, we found that the inland water emissions offset the carbon uptake capacity of the plants by 9%–13%. This effect was mainly driven by emissions of methane and carbon dioxide—nitrous oxide emissions played a minor role. Our study shows that greenhouse gas emissions from Arctic lakes, ponds, and streams are an important part of the carbon exchange between the land and atmosphere.

Key Points:

- Integrating carbon emissions from inland waters into the carbon landscape exchange offset the summer terrestrial carbon sink by ∼9–∼13%.
- Carbon emissions from inland waters were higher during floods compared to nonflood conditions.
- When nitrous oxide emissions were included as carbon dioxide equivalents, these emissions were negligible relative to carbon emissions.

Supporting Information:

Supporting Information may be found in the online version of this article.

Correspondence to:

M. Martyn Rosco,
m.martynrosco@vu.nl

Citation:

Martyn Rosco, M., Dean, J. F., Borges, A. V., Meisel, O. H., van Logtestijn, R., Hensgens, G., et al. (2025). The importance of inland water CO_2, CH_4, and N_2O for summertime greenhouse gas exchange with the atmosphere in Arctic tundra lowlands. *Journal of Geophysical Research: Biogeosciences*, *130*, e2024JG008334. https://doi.org/10.1029/2024JG008334

Received 25 JUN 2024
Accepted 3 JUN 2025

Author Contributions:

Conceptualization: Melanie Martyn Rosco, Joshua F. Dean
Data curation: Melanie Martyn Rosco, Joshua F. Dean, Geert Hensgens
Formal analysis: Melanie Martyn Rosco, Geert Hensgens
Funding acquisition: Joshua F. Dean, A. Johannes Dolman
Investigation: Melanie Martyn Rosco, Joshua F. Dean, Alberto V. Borges, Ove H. Meisel, Richard van Logtestijn, Sergei Karsanaev, A. Johannes Dolman
Methodology: Melanie Martyn Rosco, Alberto V. Borges

1. Introduction

Inland waters, such as ponds, lakes, and fluvial systems, are common features of Arctic tundra landscapes, with carbon and nutrient cycles that are closely coupled to terrestrial processes (Kling et al., 1991). Terrestrial organic material that enters inland waters can be transported, sequestered in sediments, and subjected to biogeochemical transformation processes (Drake et al., 2018). Riparian wetlands also provide inorganic and organic carbon to inland waters. As a result of both terrestrial and wetland subsidies, inland waters are important emitters of the greenhouse gases (GHGs) carbon dioxide (CO_2) and methane (CH_4), and to a lesser extent nitrous oxide (N_2O), to the atmosphere (Hu et al., 2016; Raymond et al., 2013; Rosentreter et al., 2021). In the Arctic, the terrestrial organic

Project administration: Joshua F. Dean, Trofim Maximov, A. Johannes Dolman
Resources: Joshua F. Dean, Alberto V. Borges, Richard van Logtestijn, Rien Aerts
Supervision: Joshua F. Dean, James T. Weedon, Jorien E. Vonk, A. Johannes Dolman
Validation: James T. Weedon
Visualization: Melanie Martyn Rosco
Writing – original draft: Melanie Martyn Rosco
Writing – review & editing: Melanie Martyn Rosco, Joshua F. Dean, Alberto V. Borges, Ove H. Meisel, Geert Hensgens, James T. Weedon

matter transformed in inland waters is composed of primarily contemporary carbon fixed from the atmosphere within the last century (Dean et al., 2020; Elder et al., 2018; Raymond et al., 2007). However, older and previously sequestered soil organic matter is increasingly vulnerable to remobilization and degradation due to permafrost thaw (Biskaborn et al., 2019), driven by amplified warming in the northern high latitudes (Hensgens et al., 2021; Meredith et al., 2019; Schwab et al., 2020). Approximately half of the global soil organic matter is stored in the upper 3 m of Arctic permafrost soils, containing an estimated 1,300 Pg of carbon (Hugelius et al., 2014) and 67 Pg of nitrogen (*N*) (Harden et al., 2012). Therefore, permafrost thaw could result in a potentially large, yet poorly constrained, feedback to ongoing climate change (Dean et al., 2018; Schuur et al., 2015; Voigt et al., 2017).

While high-latitude inland waters are generally net carbon emitters, the contribution of CO_2 and CH_4 emissions from inland water to landscape carbon exchange with the atmosphere is poorly quantified (Denfeld et al., 2013; Karlsson et al., 2021; Lundin et al., 2013). GHG emissions from Arctic inland waters typically show high degrees of spatial and temporal variability, driven by local environmental and climatic factors. Relatively few direct observations of these emissions exist, especially in the remote northeast lowlands of the Siberian Arctic (ca. 493,000 km^2) where ponds, lakes, and fluvial systems are widespread features and soils are estimated to contain 100 Pg of carbon (Grosse et al., 2013; Muster et al., 2017; Nitzbon et al., 2020). Inland water coverage in Arctic lowland landscapes is highly variable (Grosse et al., 2008) and can change due to drainage of water bodies (Jones & Arp, 2015) or ground subsidence driven by permafrost thaw and shifts in local topography (Liljedahl et al., 2016; Vonk et al., 2015). Understanding the distinct contributions of ponds, lakes, and fluvial systems is crucial because these water bodies exhibit different hydrological, biogeochemical, and emission dynamics. By differentiating between these systems, we can more accurately assess their individual roles, which will allow for a better balancing of regional carbon budgets (Webb et al., 2019), in addition to improving estimates of future emissions.

The Arctic has generally low availability of nitrogen (*N*), partially due to low atmospheric deposition (Dentener, 2006) and partially due to high competition between microbes and vegetation for the available *N* (Jonasson et al., 1999). Thus, N_2O emissions from Arctic landscapes and their inland waters have received less attention than those of CO_2 and CH_4 (Martikainen et al., 1993; Rodionow et al., 2006). High N_2O emissions have been recorded from subarctic bare peat surfaces after permafrost thaw (2.81 ± 0.6 mg N_2O m^{-2} d^{-1}, Voigt et al., 2017). However, inland waters tend to be either minor N_2O sinks or sources (Harms et al., 2020; Kortelainen et al., 2020; Soued et al., 2016). This was also observed in other low *N* inland water environments such as the Congo River (Borges et al., 2019). The uncertain role of inland waters in the Arctic N_2O budget makes it difficult to constrain how N_2O emissions might impact permafrost climate feedbacks.

One possible consequence of a warming Arctic is the risk of increased flooding of lowland tundra landscapes. Deeper snow depth and longer snow cover duration have already been observed in Siberia (Bulygina et al., 2011), whereas climate models predict continued increases in snow depth during this century (Callaghan et al., 2011; Thackeray et al., 2019). This means greater meltwater runoff in the spring, resulting in increased magnitude and/or duration of flood events. Flooding can increase inland water emissions as observed in other Siberian rivers (Krickov et al., 2021; Vorobyev et al., 2021). In northeast Siberia, an additional ~250% of precipitation fell in autumn 2016 (as snow) compared to the average of the previous 11 years. This increased snowfall resulted in the Indigirka River spring melt runoff lasting from May until mid-July 2017 compared to its usual abatement in June (Iwahana et al., 2014; Tei et al., 2020). The high runoff caused extreme flooding, which increased the inundated area of the Indigirka River lowlands from 10,789 km^2 in July of 2015 to 16,016 km^2 in July of 2017, a ~50% increase (Tei et al., 2020).

Quantifying GHGs (CO_2, CH_4, and N_2O) emissions from different types of inland waters in a range of hydrological conditions in the context of the terrestrial sink demonstrates the potential importance of inland waters to regional GHGs budgets. Here we present simultaneous concentration measurements of dissolved CO_2, CH_4, and N_2O from ponds, lakes, and low-order fluvial systems in the Indigirka River lowlands in northeast Siberia across two summers (2016 and 2017). Our field campaigns included the tail end of the May–July 2017 flood event. The measured concentrations were used to calculate diffusive CO_2, CH_4, and N_2O emissions to the atmosphere and their relative magnitude to terrestrial emissions during a flood (2017) and nonflood year (2016). The objectives of this study were to quantify the following: (a) the importance of daily CO_2-C and diffusive CH_4-C emissions from all inland water types present in comparison to the combined terrestrial CO_2-C and diffusive CH_4-C exchange of the study area; (b) the importance of inland water N_2O emissions relative to CO_2 and CH_4 emissions; and (c) the impact of flooding on the landscape GHG exchange with the atmosphere.

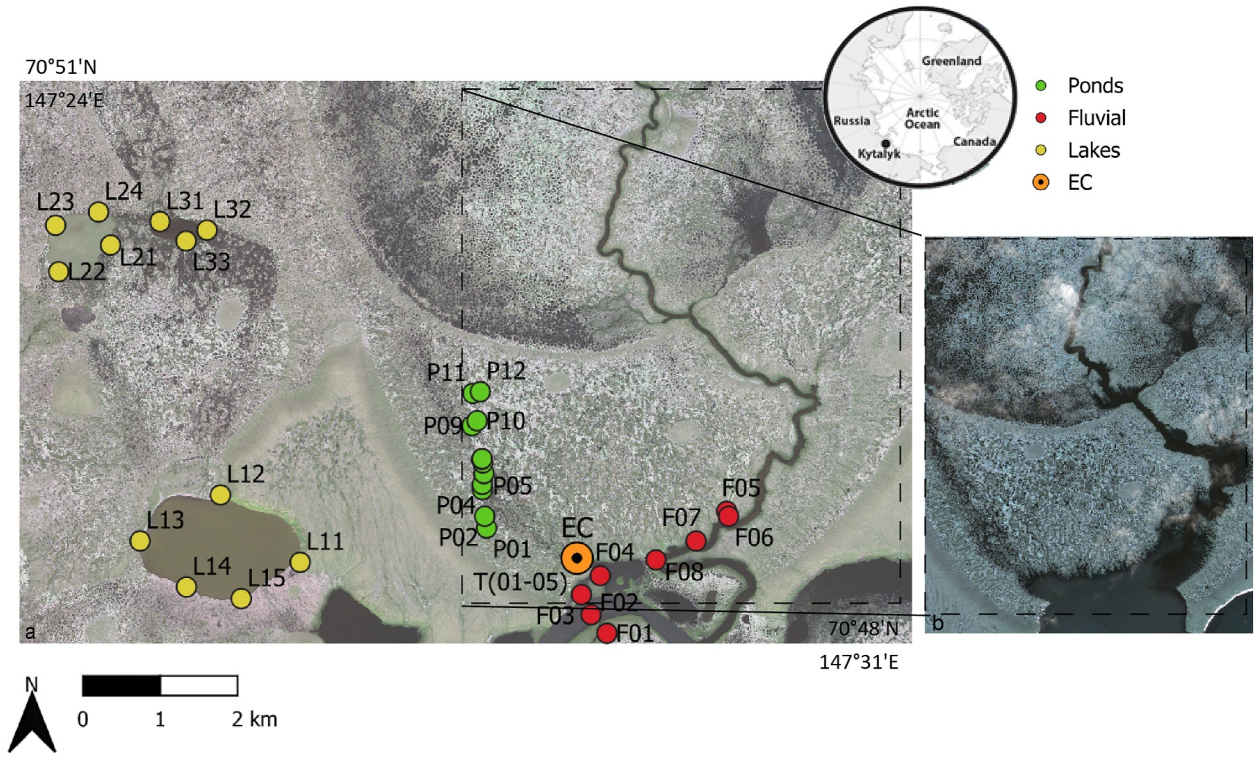

Figure 1. (a) Kytalyk research area shown in the WorldView-2 image from July 2015. The image shows the study area over which the landscape greenhouse gas exchange was determined (17.81 km^2). (b) This panel shows the flooding extent in the WorldView-2 image from July 2017—the left half of the image was obscured by cloud cover and therefore was excluded in this image and not used in our analysis. The box outlined with dashed black lines in panel (a) indicates the area covered by the image in panel (b). Flood samples were taken by the Eddy Covariance (EC) tower and are indicated with T (01–05). EC marks the location of the EC tower.

2. Materials and Methods

2.1. Study Area

The "Kytalyk" National Park is located in the Indigirka Lowlands, Sakha Republic, northeast Siberia (70°49′N, 147°29′E). The study area occupies ∼18 km^2 on the north bank of the Berelekh River, a western tributary to the Indigirka River, 30 km northwest of the town Chokurdakh (Figure 1). The broader Indigirka River basin encompasses approximately 120,610 km^2 (Tei et al., 2020). Our study area lies within the lower Indigirka floodplain, where hydrological boundaries are often diffuse and not well defined, particularly in thermokarst-affected landscapes with none to minimal gauging infrastructure. The region is underlain by continuous permafrost over 300 m thick (Shahgedanova, 2003) with an overlying active layer that thaws ∼20–30 cm deep every summer during July/August (Dean et al., 2020). The local climate is continental, with a mean annual air temperature of −13.4°C and an average July temperature of 10.3°C (1981–2010) (Trouet & Oldenborgh, 2013). The mean annual precipitation is ∼230 mm, of which roughly half falls as rain during the growing season (May–September) and the other half as snow (Dean et al., 2020). Snowmelt usually begins at the end of May to early June (Iwahana et al., 2014). The landscape is dominated by three topographical levels, from lowest to highest: river floodplain areas, drained thermokarst lake basins of Holocene age (alases), and ridges of Pleistocene-aged sediments termed yedoma. The local vegetation is classified as graminoid tundra: tussock sedge, dwarf shrub, and moss tundra (Walker et al., 2005).

2.2. Study Approach

In the interest of clarity throughout this study, we briefly define the terminology used here. In this study, we define "C emissions" as the combined daily CO_2-C and diffusive CH_4-C, whereas GHG emissions are defined as the combined CO_2, CH_4, and N_2O emissions in CO_2 equivalents:

$$\text{C emissions} = CO_2\text{-C} + \text{diffusive } CH_4\text{-C per day}$$

$$\text{GHG emissions} = CO_2 + CH_4 + N_2O \text{ per day}$$

When discussing the dissolved gas concentrations, we refer to 2016 as a "normal" year and 2017 as a "wet" year:

$$\text{Normal year} = 2016 \text{ dissolved gas concentrations}$$

$$\text{Wet year} = 2017 \text{ dissolved gas concentrations}$$

The flooding that occurred in 2017, mainly along the extended riparian zone of the Berelekh River, did not reach the northernmost two lakes (L21–L24, L31–L33) and ponds (Figure 1). Nonetheless, the influence of the higher snowfall from the previous autumn (2016) is reflected in the observed measurements (see Section 3 and Section 4). In the upscaling results and discussion, we refer to a nonflood and a flooded scenario. In the flooded scenario, we include floodwaters (Figure 1b) as a separate inland water system to discern their effects on upscaled emissions (see also Section 2.7).

$$\text{Non-flood scenario} = \text{all inland water systems included in upscaling}$$

$$\text{Flooded scenario} = \text{all inland water systems} + \text{floodwater as conceptual inland water system included in upscaling.}$$

2.3. Sampling

Inland water sites were sampled in summer (late July to early September) of 2016 and 2017. In total, two small lakes (<3 m deep, 0.04 and 0.14 km^2 in area), one thermokarst lake (L11–L15, up to 7 m deep, 0.51 km^2, actively eroding into a yedoma ridge), 12 pond sites (<0.5 m deep, 3–240 m^2), and 8 fluvial sites along a ∼5-m-wide stream and the Berelekh River bank were sampled (Figure 1). Due to the logistical challenges of site access in the far east Siberian Arctic tundra at the Kytalyk Nature Reserve, water bodies could only be accessed by foot. Therefore, sampling of dissolved concentrations could only be obtained by syringe headspace equilibrations, and direct flux measurements were not possible. Further, water bodies could only be sampled from the edge (Dean et al., 2020). Lake areas were derived from a geomorphological map of the study area (van Huissteden et al., 2021), whereas pond surface areas and stream width were measured in the field with tape measures and are indicative. Additionally, five locations of flooded tundra area were sampled in 2017. For an overview of the sampling locations and frequency, please see Table S1 in Supporting Information S1. Ponds are defined in this study as lentic water bodies with a surface area smaller than 0.01 km^2. Each flooded tundra location was sampled four times in 2017. In situ measurements of water temperature, pH, electrical conductivity (EC), water depth, and surface area were performed during sample collection. Temperature and EC were measured with a Greisinger GMH 3431 m (accuracy of ±2 µs/cm and ±0.2 K); pH was measured using a Sensorex SAM-1™ m (accuracy of ±0.01). EC values were converted to freshwater salinity values using a factor of 0.55 (Rusydi, 2018). Dissolved gas samples from the surface water and ambient air samples were collected using the headspace technique following Borges et al. (2015) and Dean et al. (2020). Surface water was collected directly using a 60-mL polypropylene syringe, which was prerinsed three times with sample water before collection. Water was drawn gently from 5 to 10 cm below the surface to minimize turbulence and bubble formation. Samples were equilibrated in 60-mL syringes by shaking 30 mL water with 30 mL ambient air for 1 min, away from direct sunlight. After equilibration, the headspace was transferred to a pre-evacuated 12 mL Exetainer® vial (Labco, UK).

2.4. Greenhouse Gas Analyses

Headspace GHG concentrations were determined using an SRI 8610C gas chromatograph (GC) at the University of Liège. CO_2 and CH_4 concentrations were measured by a flame ionization detector fitted with a methanizer, and N_2O concentrations were measured by an electron capture detector equipped in the GC. The GC was calibrated with CH_4:CO_2:N_2O mixtures (Air Liquide Belgium) of 1, 10, and 30 ppm CH_4, 400, 1,000, and 4,000 ppm CO_2; and 0.2, 2.0, and 6.0 ppm N_2O. The concentrations of CO_2, CH_4, and N_2O were calculated according to Henry's

law using solubility coefficients from Weiss (1974), Yamamoto et al. (1976), and Weiss and Price (1980), respectively.

2.5. GHG Flux Calculations

The GHG fluxes (F) between the water surface and atmosphere were calculated according to Fick's first law:

$$F = k(c_{\text{surf}} - c_{\text{eq}}) \tag{1}$$

where k is the gas exchange constant (cm h^{-1}), c_{surf} is the gas concentration in surface water (μmol L^{-1}), and c_{eq} is the gas concentration in surface water in equilibrium with the atmosphere (μmol L^{-1}). Daily average atmospheric gas concentrations were determined from ambient samples taken throughout the sampling campaign. In 2016, no N_2O ambient air samples were available, and in 2017, no CO_2 ambient air samples were available. In these instances, monthly averages were used from discrete flask measurements taken at the NOAA Hydrometeorological Observatory of Tiksi, Russia (~300 km away from the field site) (Dlugokencky et al., 2015).

The gas exchange constant k was computed by normalizing the gas transfer velocity to the Schmidt number of 600, which corresponds to the Schmidt number of CO_2 at 20°C in freshwater.

$$k = k_{600}\left(\frac{Sc}{600}\right)^{-b} \tag{2}$$

Here, b is the Schmidt exponent; $b = 0.67$ for wind speeds <3 m s^{-1} and $b = 0.5$ for wind speeds ≥3 m s^{-1} (Jähne et al., 1987). Sc is the Schmidt number of the gas, calculated from empirical fourth-order polynomial fits of Schmidt number versus water temperature (Wanninkhof, 2014). K_{600} was calculated using a power relationship between wind speed at a height of 10 m and gas exchange determined for low wind environments (Cole & Caraco, 1998):

$$k_{600} = 2.07 + 0.215 \times U_{10}^{1.7} \tag{3}$$

where wind speed per day was the average of all measurements taken by the local meteorological tower, gap-filled with ERA5 data (Hersbach et al., 2020), every 30 min between 9:00 and 17:00 (Dean et al., 2020). The power law was used to convert the measurements taken at a height of 5 m (U_r) to corresponding wind speeds at a 10-m height (U_{10}):

$$U_{10} = U_r \times \left(\frac{10}{z_r}\right)^{a} \tag{4}$$

Where the exponent a quantifies wind shear and for near-neutral stability conditions over land, a is approximately $\frac{1}{7}$, and z_r is the reference height at 5 m. Finally, values are averaged to provide daily wind speed values.

Equation (3) was used to derive k_{600} values for lake fluxes and floodwater fluxes, as the floodwater was characterized by standing water with large surface areas equivalent to a lake (Figure 1b). The power relationship does not always apply consistently for ponds and fluvial systems. For ponds, five k_{600} values were found in the literature (Holgerson et al., 2017; Kuhn et al., 2018). For fluvial systems, two values were found in the literature (Aufdenkampe et al., 2011; Denfeld et al., 2013), and two values were derived from a parameterization as a function of stream slope and velocity (Raymond et al., 2012), with stream slope values taken from RiverATLAS (Linke et al., 2019) and stream velocity computed from discharge (Liu et al., 2022). For a list of the aforementioned k_{600} values, please see Table S2 in Supporting Information S1. To account for the possible range in k_{600} values in pond and fluvial sites, a uniform distribution containing 1,000 values, to represent the equal likelihood of each value, was generated from the literature values. Values from the corresponding distribution were randomly assigned to each sample to estimate a nonbiased k_{600} value.

2.6. Inland Water Surface Area Coverage Calculations

In order to estimate inland water emissions, the surface area coverage is needed in addition to the fluxes of each inland water system. The relative area coverage of ponds, fluvial systems, and the tundra was derived by classifying an available WorldView-2 satellite image with a 2-m spatial resolution and four spectral bands (blue, green, red, and near infrared) from the 10th of July 2015. We estimated from visual corroboration during fieldwork that water surface area coverage in 2016 was similar to that in 2015. Polygons of the lake areas from a geomorphological map of the study area (van Huissteden et al., 2021) were used to mask out the lakes in the satellite image. Digital numbers in the remote sensing products were converted to radiance values and subsequently to top-of-atmosphere reflectance values. A random forest (RF) classification model (Breiman, 2001) was used (*scikit-learn* package; Pedregosa et al., 2011) in Python version 3.11.6 (Van Rossum & Drake, 2009) to classify pixels either as pond, fluvial, or tundra classes. Training data were generated by visual inspection; 1,000 points were selected for each class. The out-of-bag (OOB) error is derived in a bootstrapping procedure using about one-third of the data and provides an unbiased estimate of the model performance (Breiman, 2001). The OOB prediction of accuracy for the 2015 image classification was 99.4%. Single pixels were sieved to remove noise. We set a limit of each water body consisting of at least two pixels, which equates to a surface area of 16 m^2: Only one sampled pond (P06) had a surface area smaller than this, which is discussed further in Section 3 and subsection 4.1.1.

To analyze the effect of tundra flooding on the landscape's GHG exchange, the calculation of inland water area coverage assumed that the flooded tundra area was the difference in water surface area coverage between the cloud-free segment of a WorldView image from the 9th of July 2017 and the image from 2015 (Figure 1b). The 2015 image represents a "normal" year with no extreme flooding, and it serves as the baseline for comparison with the 2017 flood event. The fluvial surface area coverage was assumed to be the same in 2017 as in 2015 and is considered separately from the flooded tundra in the flooded-scenario upscaling calculations described below (Section 2.7) in order to isolate the effect of the additional flooded area separate from the usual fluvial surface area coverage (i.e., the floodwaters are considered their own inland water "type" in addition to the ponds, lakes, and existing fluvial system). RF classification on the WorldView image from the 9th of July 2017 was carried out with its own 1,000-points-per-class training data set and yielded an OOB prediction accuracy of 86.5%.

2.7. Landscape GHG Exchange Calculations

The CO_2 and CH_4 flux of the tundra land cover class is derived from measurements recorded by an EC tower during the 2016 sampling period (31 July 2016–09 August 2016) (Dean et al., 2020). Eddy covariance measurements were only available for 2016. The tower site was flooded during summer 2017, which disrupted instrumentation and prevented data collection that year. The eddy covariance (EC) tower was installed in 2003 and is outfitted with an ultrasonic anemometer (Gill Instruments, Lymington, UK, R3-50) for measuring wind speed and temperature and two open-path infrared gas analyzers for the measurements of CO_2 (LI-COR LI-7500) and CH_4 (LI-COR LI-7700). The methane analyzer was initially installed in 2008 and was upgraded to the model mentioned above in 2014. All measurements are collected at 10 Hz at a height of 4.7 m. The footprint of the tower has a diameter of approximately 300 m. Method validation of the EC methods was demonstrated at the site previously (Dean et al., 2020).

Data were processed using EddyPro (version 6.2.2) software and transformed to 30-min flux averages. The configuration was set to include 2D rotation of anemometer coordinates, WPL correction (compensation of air density variations), spectroscopic corrections for the LI-7700, and spectral corrections. Data quality was ensured by removing values that did not pass the EddyPro quality control and implausibly high fluxes. Subsequent filtering was done by removing fluxes with too low air friction ($u^* < 0.163$). Spikes were removed only for CO_2 fluxes following a standardized method, using a threshold z of four over a period of 13 days (Papale et al., 2006).

Only fluxes measured during the day, between 09:00 and 17:00, were selected to match that the dissolved gas concentrations were only sampled during the day. Additionally, only fluxes captured from a wind direction covering a dry or mixed area that did not contain the river are used, as open water covers less than 1% of these areas in the study site (Parmentier et al., 2011). Tundra N_2O fluxes (48 in total) are selected from aggregated data published by Voigt et al. (2020) if they matched the following criteria: measured in situ in Arctic and subarctic regions, either on upland or peatland ecosystems, on vegetated or partly vegetated surfaces, without disturbance or experimental manipulation.

To evaluate the contribution of CH_4 and N_2O emissions to the daily inland water GHG emissions and daily landscape GHG exchange with the atmosphere, CH_4 and N_2O were converted to CO_2 equivalent using sustained global warming (SGWP) and cooling potentials (SGCP) over a 100-year timeframe (Neubauer & Megonigal, 2015) (CH_4: SGWP = 45, SGCP = 203; N_2O: SGWP = 270, SGCP = 349).

To calculate the daily GHG and C fluxes for each inland water system and to estimate associated uncertainties, we followed a nonparametric bootstrapping procedure (Efron, 1987). First, outliers in c_{surf}, identified following the 1.5 interquartile range rule, were excluded from the flux calculations. For each water system, we generated 1,000 k, c_{surf}, and c_{eq} by values by sampling with replacement from the data observed or computed (as detailed above), and calculated the median of each bootstrap sample. This resulted in 1,000 values of each parameter, which were then used to compute a corresponding distribution of flux estimates by Equation 1. The same method was applied to tundra GHG and C fluxes, also 1,000 times. The median GHG and C flux was multiplied by the corresponding water surface area coverage to calculate daytime summer GHG and C diffusive emissions per day. In 2017, when the floodwater fluxes were included, fluvial and floodwaters were considered separate classes. Daily landscape GHG or C exchange, the sum of tundra emissions and inland water GHG or C diffusive emissions, was calculated for the study area (17.81 km^2; Figure 1).

We used the standard rules of error propagation to quantify uncertainty in resulting emissions (Karlsson et al., 2021; Serikova et al., 2019). We assumed 15% uncertainty in the water areas, 15% being a conservative estimate based on the OOB values from the RF classifications:

$$\delta R_i = R \times \sqrt{(\delta x)^2 + (\delta y)^2}$$

Here, δR_i is the uncertainty of GHG/C emissions for each inland water system or the tundra, R is the mean calculated emission, δx is the coefficient of variation of the emission, and δy is the 15% uncertainty estimate of surface areas. Then the uncertainties for the total inland water GHG/C emissions and landscape GHG/C exchange are estimated as follows:

$$\delta R_{total} = \sqrt{\sum (\delta R_i)^2}$$

Here, δR_{total} is the uncertainty of the total inland water GHG/C emissions or landscape GHG/C exchange, and δR_i are GHG/C emissions uncertainties for each inland water system or the tundra. The upscaled emissions and the corresponding uncertainties are reported as a mean ± 1 SD.

2.8. Statistical Analysis

To investigate the spatiotemporal variability and autocorrelation of the dissolved gas concentrations from lake and pond samples, we used a linear mixed model (LMM) with random effects in R version 4.1.3 (R Core Team, 2019) using the *lme4* package (Bates et al., 2015). Sampling years and sampling sites are set as random effects. Model assumptions were verified by plotting residuals versus fitted values to check homogeneity and plotting residuals versus theoretical values from a normal distribution on a q-q plot to check normality (Zuur et al., 2009). No fixed effects were set because the model is used only to analyze spatiotemporal variance by implementing random effects; therefore, the assumption of multicollinearity was not checked. There were insufficient fluvial data to run an insightful LMM analysis due to inconsistencies in the locations of sample sites caused by the flooding in 2017.

Note that in the text we report measured values including outliers. When reporting measured variables and uncertainty, we used median [interquartile range] due to the nonnormal distribution of the data.

3. Results

All sampled inland waters were supersaturated with CO_2 and CH_4 with respect to atmospheric concentrations (Figures 2 and 3). Dissolved CO_2 concentrations ranged from 27 to 1,333 μmol L^{-1} and dissolved CH_4 from 0.04 to 251 μmol L^{-1} (Table 1). Ponds generally had the highest concentrations, followed by fluvial and then lake sites (Figures 2 and 3). CO_2 concentrations at pond sites were ∼9 and ∼3-fold greater than at lake and fluvial sites,

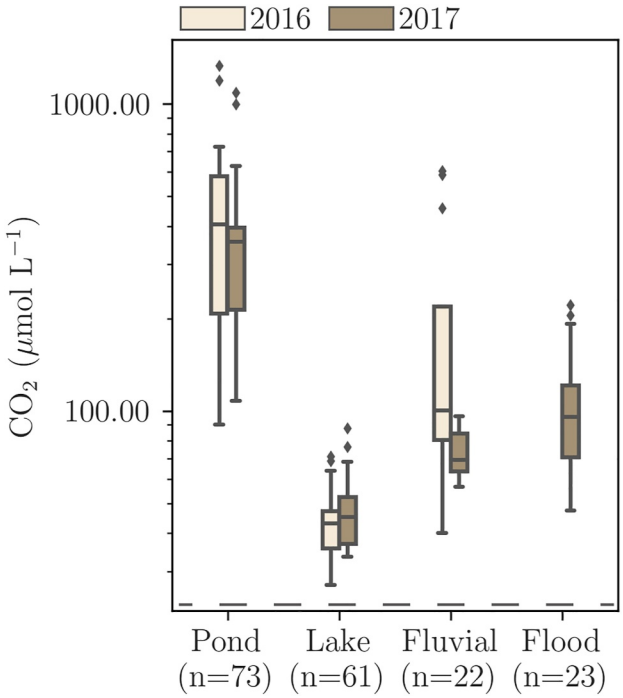

Figure 2. CO_2 surface water dissolved concentrations from ponds, lakes, fluvial, and flood sites in Kytalyk, Siberia in 2016 and 2017. The dashed line at the bottom of the panel indicates the mean atmospheric concentrations in equilibrium with the atmosphere, CO_2 = 19 µmol L^{-1}. The boxes indicate the interquartile range, and the whiskers indicate the 1.5 × interquartile range. Dots indicate values that lie outside the 1.5 × interquartile range. Note the *y*-axis is in log scale. N values in the brackets indicate the sample number.

respectively. The difference between pond CH_4 concentrations and lake and fluvial sites was even higher (~25-fold and ~4-fold, respectively; Figure 3).

The variance of pond CO_2 and CH_4 concentrations was, according to the linear mixed model (LMM; see Methods Section 2.7), as much explained by the spatial variance between ponds (42% and 58% of total variance, respectively) as by variance within a pond and year (49% and 59%, respectively). The highest pond CO_2 and CH_4 concentrations were found in P06 (median 1,041 [IQR 793–1,163] µmol L^{-1} and 151 [73–225] µmol L^{-1}), which is the smallest sampled pond with a subpixel surface area of 3 m^2. As a result of these high values, site P06 was excluded from the LMM analysis. This pond appears to have formed within a melting ice wedge (Figure S1A in Supporting Information S1).

For lake concentrations, the variance of CO_2 and CH_4 concentrations between sampling sites within a lake was higher (35% and 4%, respectively) than the variance between lakes (3% for CO_2 and 5% for CH_4). These results indicate no significant variance between dissolved gas concentrations from different lakes. In the LMM, with the spatial random effect set as the sampling sites within a lake, a much lower proportion of the total variance in lake dissolved gas concentrations was explained by variation between the sampling years for CO_2 concentrations (13%) in comparison to CH_4 concentrations (79%).

Dissolved CO_2 and CH_4 concentrations had the largest variation at fluvial sites (Figures 2 and 3), in part due to the highest CO_2 and CH_4 concentrations found at site F05 (588 [522–596] µmol L^{-1}, 42 [29–51] µmol L^{-1}, respectively); these values were an order of magnitude for CO_2 and two orders of magnitude for CH_4 higher than those of all other fluvial sites (75 [65–90] µmol L^{-1}, 0.5 [0.4–1.7] µmol L^{-1}). Site F05 was categorized as a fluvial site as it appears on satellite images to be a small channel joining the stream. The field campaign revealed that F05 was largely disconnected from the main channel that joins the stream (Figure S1B in Supporting Information S1). It is unclear if F05 was a pond that connects to the stream when overland flow occurs or if it had become disconnected over time. A quantitative analysis of fluvial CO_2 and CH_4 concentration variances was not possible due to the logistical disruption caused by the flooding in 2017, making the sites sampled in 2016 inaccessible. As a result, none of the same fluvial sites were sampled in both years. Nonetheless, visual inspection of Figures 2 and 3 indicates that CO_2 and CH_4 concentrations were lower in 2017 than in 2016, especially for CH_4 concentrations.

Given the lack of consistent spatial patterns in lake CO_2 and CH_4 concentrations and the approximately equal within- and between-pond variability, we combined data from each inland water type within a sampling year for the upscaling analysis. Temporal differences were clearer for CH_4 than for CO_2 (Figures 2 and 3), but this variation did not warrant treating sites separately within an inland water type. As a result, we defined one representative land cover class per inland water type (lake, pond, fluvial) for each year. This resulted in a single lake, pond, and fluvial land cover class for 2016 and 2017. The impact of flooding on fluvial CO_2 and CH_4 concentrations is taken into consideration through the upscaling exercise by accounting for a nonflood summer scenario using concentration values from 2016 only and a separate upscaling for a flooded summer scenario using concentration values from 2017 (see Section 2.2).

3.1. CO_2 and CH_4 Emissions and Upscaling

The estimated C emissions (defined as the combined daily CO_2-C and diffusive CH_4-C in subsection 2.2) from all inland waters across the study area in the nonflood summer scenario were 7.03 ± 1.30 Mg C d^{-1} (mean ± SD). Ponds had the largest surface area coverage (10%) of the different inland water systems (Table 1) and the largest contribution to inland water C emissions with 5.13 ± 1.24 Mg C d^{-1} (73%), fluvial systems were the second largest contributors with 1.40 ± 0.38 Mg C d^{-1} (20%), and lakes contributed 0.50 ± 0.09 Mg C d^{-1} (7%). CO_2-C accounted for the majority of inland water C emissions (97%) in contrast to CH_4-C (3%). Tundra emissions were −83.35 ± −13.30 Mg C d^{-1} for CO_2 and 0.54 ± 0.11 Mg C d^{-1} for CH_4-C resulting in a landscape C exchange

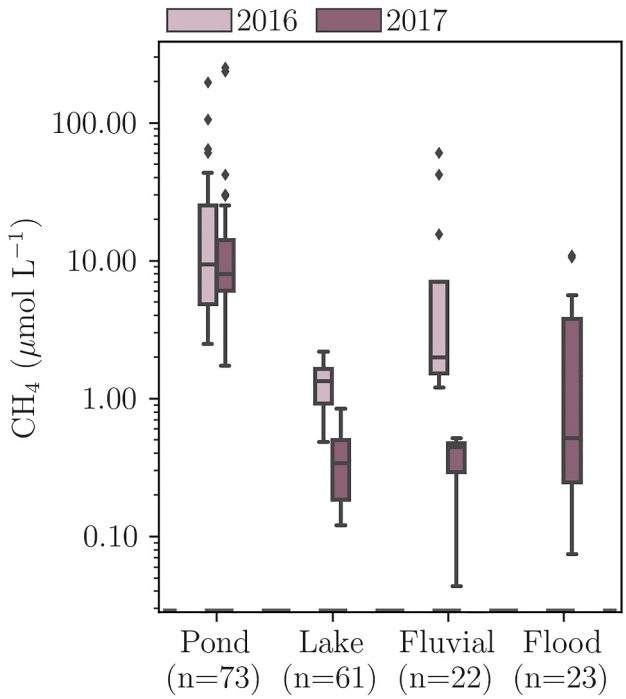

Figure 3. CH_4 surface water dissolved concentrations from ponds, lakes, fluvial, and flood sites in Kytalyk, Siberia in 2016 and 2017. The dashed line at the bottom of the panel indicates the mean atmospheric concentrations in equilibrium with the atmosphere, $CH_4 = 0.004$ µmol L^{-1}. The boxes indicate the interquartile range, and the whiskers indicate the 1.5 × interquartile range. Dots indicate values that lie outside the 1.5 × interquartile range. Note the *y*-axis is in log scale. N values in the brackets indicate the sample number.

with the atmosphere of −75.78 ± 13.29 Mg C d^{-1}. Lakes account for less than 1% of total landscape C exchange, fluvial systems for 2% and ponds for 7%. Including C emissions from the inland waters offsets the landscape C sink by around 9%.

3.2. N_2O Emissions and Upscaling

In 2016, the pond, lake, and fluvial sites were undersaturated with N_2O with respect to the atmosphere, whereas in 2017, the wet year, lake and fluvial sites became oversaturated, while pond and flood N_2O concentrations ranged from undersaturation to oversaturation (Figure 5). Pond N_2O concentrations were, on average, the lowest of the four inland water systems. The LMM analysis showed that the variance between sampling years explained much of the variance observed in N_2O concentrations in ponds (68% of total variance) and lakes (95%).

In the nonflood summer scenario, CO_2 emissions accounted for 70%, and diffusive CH_4 emissions for 31%, of the inland water GHG emissions in CO_2 equivalents; N_2O emissions acted as a net weak sink, reducing the net radiative forcing of inland water emissions by the equivalent of <1%. Integrating inland water N_2O emissions with the tundra, which acted as a N_2O source, resulted in N_2O emissions offsetting the net radiative forcing of the landscape GHG sink by the equivalent of ∼0.1%.

The tundra was a CH_4 source ($3 \pm 1 \times 10^4$ kg $CO_{2\text{-eq}}$ d^{-1}), which, due to its large warming potential, offset the tundra GHG sink by 10%. However, because the tundra was a large CO_2 sink ($-30 \pm 5 \times 10^4$ kg $CO_{2\text{-eq}}$ d^{-1}), this part of the landscape continued to act as a net GHG sink ($-28 \pm 5 \times 10^4$ kg $CO_{2\text{-eq}}$ d^{-1}). The additional net radiative forcing of inland water GHG emissions ($4 \pm 1 \times 10^4$ kg $CO_{2\text{-eq}}$ d^{-1}) does offset the tundra GHG sink, but the landscape GHG exchange in $CO_{2\text{-eq}}$ remains overall a GHG sink relative to the atmosphere (Figure 6).

Table 1
Summary of Measured Physical and Biogeochemical Characteristics per Inland Water System

	Unit	Lake	Ponds	Fluvial	Flood
Individual area	m^2	511,200, 140,600, 41,720	3–240	-	-
Surface area coverage of study area	km^2	0.95	1.84	0.33	1.7
	%	5	10	2	7
Surface temperature	°C	9–17	9–22.4	9–15	8–17
		13 [10–14]	14 [11–16]	14 [10–15]	14 [10–15]
pH		4.8–9.1	4.4–7.6	4.9–7.8	4.9–6.3
		7.0 [6.3–7.8]	5.8 [5.4–6.0]	6.4 [5.7–7.2]	5.8 [5.5–6.2]
Conductivity	µS cm^{-1}	10–209	13–52	14–77	16–32
		29 [16–176]	21 [16–27]	46 [17–49]	19 [18–22]
Dissolved CO_2	µmol L^{-1}	27–87	90–1,333	40–603	47–220
		43 [36–49]	358 [208–496]	84 [66–106]	121 [71–121]
Dissolved CH_4	µmol L^{-1}	0.12–2.2	2–251	0.04–60	0.07–11
		0.8 [0.4–1.4]	9 [5–15]	1.2 [0.5–2.0]	0.5 [0.3–4]
Dissolved N_2O	nmol L^{-1}	5–16	0.1–13	3–15	9–14
		8 [7–13]	6 [4–8]	8 [6–13]	11 [11–12]

Note. Values are ranges (min–max) and median [interquartile range].

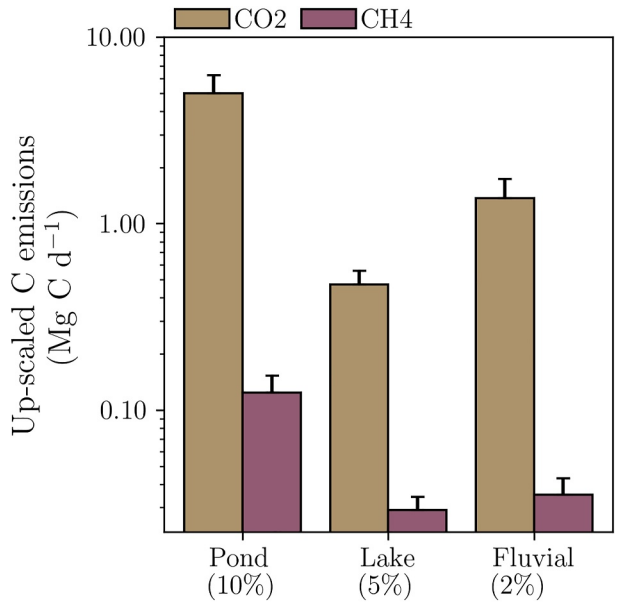

Figure 4. Estimated daily C emissions (CO_2-C and diffusive CH_4-C) per inland water system (pond, lake, and fluvial) integrated over their corresponding surface area coverage of the study area in Kytalyk, Siberia, for the nonflood summer scenario. The relative surface area (%) coverage is given in brackets. The bars represent the mean, and error bars represent the SD.

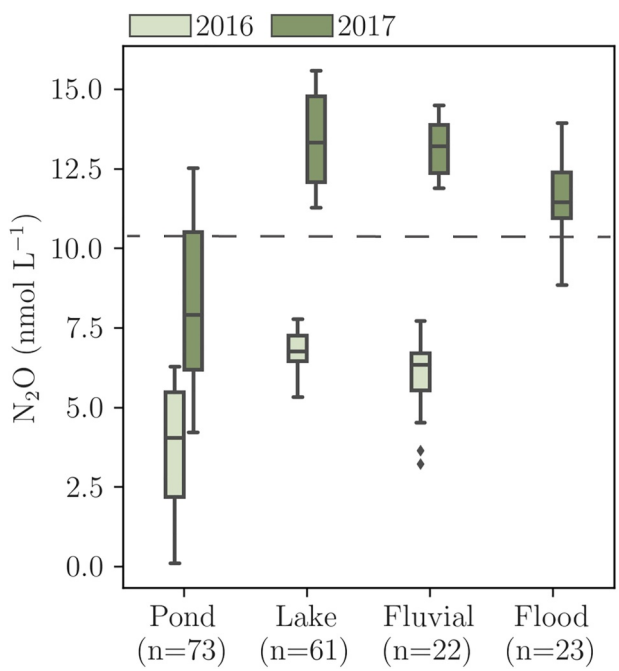

Figure 5. N_2O surface water dissolved concentrations from ponds, lakes, fluvial, and flood sites in Kytalyk, Siberia, in 2016 and 2017. The dashed line indicates the mean atmospheric N_2O concentration in equilibrium with the atmosphere = 10.77 nmol L^{-1}. The boxes indicate the interquartile range, and the whiskers indicate the 1.5 × interquartile range. Dots indicate values that lie outside the 1.5 × interquartile range. N values in the brackets indicate the sample number.

3.3. Floodwater

In 2017, an estimated 10% of our study area, previously classified as tundra, was flooded and reclassified as such. As a result, the tundra was reduced from a land area coverage of 83% down to 73% (Figure 1b). Floodwater CO_2 and CH_4 concentrations (median 96 [IQR 71–121] μmol L^{-1} and median 0.5 [IQR 0.3–3.8] μmol L^{-1}, respectively) were slightly lower than pond and fluvial concentrations but higher than in the lakes (Figures 2 and 3). We include floodwater C emissions in a flooded summertime upscaling scenario, resulting in combined CO_2-C and diffusive CH_4-C emissions from all inland waters across the study area of 9.63 ± 1.24 Mg C d^{-1} (mean ± SD), of which flood emissions accounted for 32% (Figure 7). The landscape C exchange with the atmosphere in this scenario was −63.52 ± 11.71 Mg C d^{-1}. Lake and fluvial systems and floodwaters were small N_2O emission sources in this scenario, while ponds remained small N_2O sinks, resulting in inland water N_2O emissions in CO_2 equivalents being overall a small source to the atmosphere.

4. Discussion

4.1. CO_2 and CH_4

4.1.1. Concentrations

The inland water dissolved CO_2 and CH_4 concentrations observed in this study show that ponds, lakes, and fluvial systems have markedly different carbon dynamics. The median concentrations in ponds, lakes, and fluvial systems are all significantly different from each other in both sampling years (Figures 2 and 3). Our lake sites on average had lower CO_2 and CH_4 concentrations than lakes in western Siberia (Repo et al., 2007) and Western Canada (Dean et al., 2016), but were comparable to lakes in northern Sweden (Lundin et al., 2013) (Table S4 in Supporting Information S1). Our pond CO_2 and CH_4 concentrations were similar to concentrations measured in Western Canada (Dean et al., 2016), lower than in northern Sweden (Kuhn et al., 2018), and considerably higher than an average of "temperate and boreal" ponds (Holgerson & Raymond, 2016) (Table S5 in Supporting Information S1). Fluvial CO_2 concentrations in our study area were lower than measured concentrations in northern Sweden (Lundin et al., 2013), comparable to Western Canada (Dean et al., 2016) and to streams in the Kolyma watershed (Denfeld et al., 2013). However, CH_4 concentrations at our fluvial sites were on average an order of magnitude higher than in northern Sweden (Lundin et al., 2013) and Western Canada (Dean et al., 2016) (Table S6 in Supporting Information S1). The range of flood CH_4 concentrations in this study was two orders of magnitude higher than observations in tributaries located further south to our study site, close to Chokurdakh, upstream of the Indigirka under the same flood conditions in 2017 (Morozumi et al., 2019).

We observed lower surface water CH_4 concentrations in the wet year of 2017 compared to 2016 at fluvial and lake sites. However, we did not observe this in ponds or for CO_2 concentrations. While it is likely that the deeper and longer snow cover in 2017 had an effect on CO_2 and CH_4 concentrations during the ice-cover period, it has been observed that higher precipitation in winter as snow does not have an effect on ice-free season lake CO_2 concentrations (Rantakari & Kortelainen, 2005). Ice and snow cover dynamics can affect inland water concentrations by limiting gas exchange and solar radiation, affecting the transformation processes of organic carbon into CO_2 or CH_4. It is likely that if the deeper and longer snow cover had an effect on

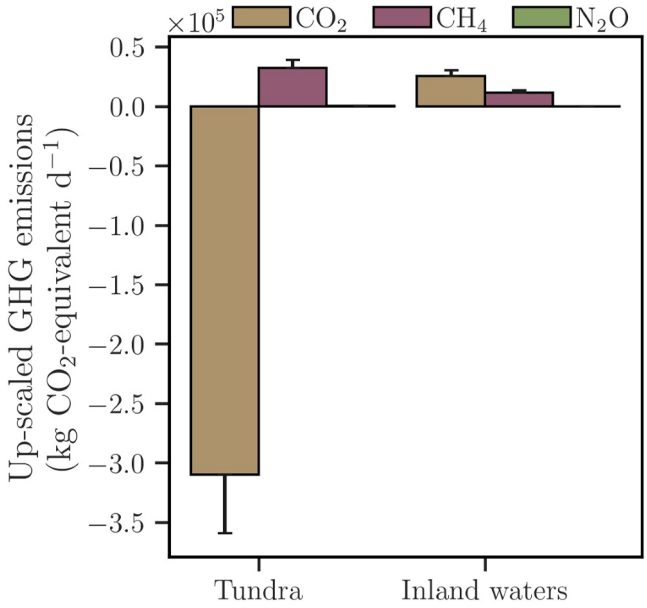

Figure 6. Estimated daily GHG (CO_2, CH_4, and N_2O) emissions of inland water and the tundra integrated over their corresponding surface area coverage of the study area in Kytalyk, Siberia, for the nonflood summer scenario. The bars represent the mean, and the error bars represent the SD. Please note that the *y*-axis is in scientific notation ($\times 10^5$).

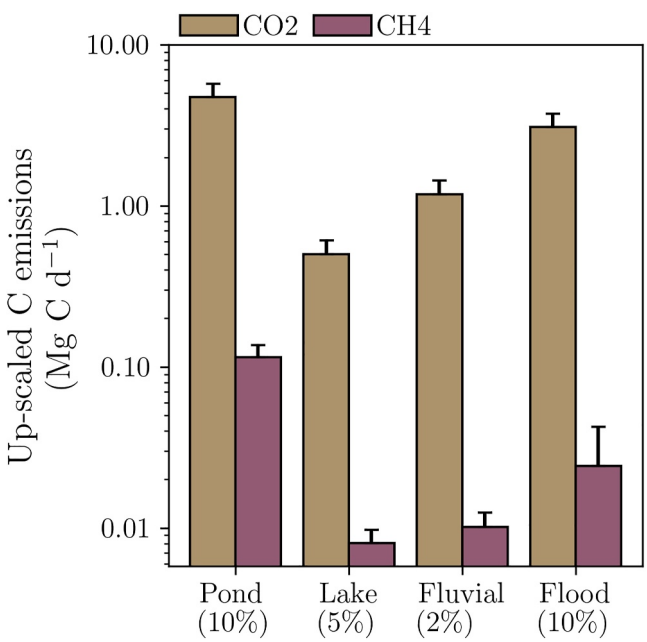

Figure 7. Estimated daily C emissions (CO_2-C and diffusive CH_4-C) per inland water system (pond, lake, fluvial, flooded tundra) integrated over its corresponding surface area coverage of the study area in Kytalyk, Siberia, for the flooded summer scenario. The bars represent the mean, and error bars represent the SD.

dissolved gases, this would have been visible for a short period at ice-off (Denfeld et al., 2015). It is more likely that lower lake and fluvial site CH_4 concentrations in the wet year are related to other environmental drivers such as temperature (Yvon-Durocher et al., 2014). We observed that lake and fluvial surface water temperatures were on average 4°C lower in 2017 compared to 2016, whereas pond temperatures were similar in both years. The lower surface water temperatures in the wet year could have been driven by the late snowmelt, and snow was still present on part of the landscape during the 2017 field campaign, whereas in ponds, the cooling effect of late snowmelt could be negated by rapid warming through solar radiation of their shallow water columns.

The high CO_2 and CH_4 concentrations measured at the smallest pond, P06, could be driven by local geomorphological features, such as its close connection to local organic carbon-rich soils due to the melting ice wedge (Holgerson, 2015; Kortelainen et al., 2006). A high degree of local connectivity with soils is also likely the reason fluvial site F05 has much higher CO_2 and CH_4 concentrations than the other fluvial sites (Harms et al., 2020). For upscaling exercises, these high-emission sites pose an interesting challenge: on the one hand, including them in the present method used for upscaling skews the values and results in high emissions that are not representative of the median emission rates. On the other hand, if several of these high emission rate sites are present in a landscape, it would appear necessary for them to be included in upscaling calculations to avoid underestimating total emissions. Thus, first a spatially extensive study into how widespread high-GHG-emitting ponds are in different landscapes is needed, followed by determining a suitable method to integrate them in upscaling exercises.

4.1.2. Upscaled Emissions

Inland water C emission contributions to C budgets and to climate forcings remain uncertain, but our results characterize inland waters in Arctic tundra lowlands as potentially important components of the landscape C exchange. In this section, we discuss the inland water C emissions (combined daily CO_2-C and diffusive CH_4-C emissions) during the studied summer months of July and August in the nonflood scenario (e.g., 2016), when inland waters covered around 3 km^2 (17%) of the study area.

Ponds dominated the inland water C emissions, contributing 73%, or 5.13 ± 1.24 Mg C d^{-1} in our study area (Figure 4). This is due to a combination of a high surface area coverage of 10% (1.8 km^2) and high CO_2 and CH_4 concentrations relative to other inland water systems both at the study site (Figures 2 and 3) and across the Arctic (Tables S3–S5 in Supporting Information S1). While our estimate of 10% pond coverage is relatively high for this part of the Arctic (Muster et al., 2017), it is not abnormally high, with similar pond coverage (12%) also observed on Samoylov Island in the Lena Delta (Abnizova et al., 2012). Determining the surface area coverage of ponds within a landscape is one of the biggest challenges in accurately quantifying their emissions. This is mainly due to their small surface areas, requiring high-resolution satellite imagery (Muster et al., 2012), and this difficulty is exacerbated by vegetation coverage. However, because ponds in Arctic lowlands contribute up to 30% of total inland water coverage (Muster et al., 2012, 2017), the potential contribution of ponds to total landscape C exchange is substantial. At the scale of our study site (~18 km^2), our estimated pond C emissions dominate inland water C emissions. It is possible that at larger scales, their contribution to the C budget is constrained by their small spatial

extent (Emmerton et al., 2016), especially in comparison to that of lakes (Rocher-Ros et al., 2017; Wik et al., 2016). It should be noted that pond emissions could become considerable contributors to the Arctic C budget once additional CH_4 evasion pathways are considered. One of these pathways is CH_4 emission through vegetation (Knoblauch et al., 2015); another is ebullition (bubbles). For example, a study in Sweden, which included CH_4 ebullition, resulted in a ∼39% reduction of a wetland C sink even though pond surface area coverage was only 4% (Kuhn et al., 2018). Thus, while our estimates can be considered conservative, the combined daily CO_2-C and diffusive CH_4-C emissions from ponds (calculated as pond C contribution = pond C emissions/landscape C exchange) still accounted for an estimated 7% of the landscape C exchange (Figure 4).

Lakes were the second-largest inland water system by area, covering 5% of the study area but only accounting for 7% of inland water C emissions. This is in agreement with observations at a similar scale (15 km^2) in northern Sweden, where lake (CO_2 and diffusive CH_4) emissions accounted for only 5% of inland water C emissions, compared to 95% by streams (Lundin et al., 2013). Again, we consider our estimates to be conservative because ebullitive CH_4 emissions were not included. Ebullition emissions have been found to range from being equivalent to diffusive CH_4 emissions in boreal peatland lakes (Kuhn et al., 2021) to accounting for the majority of lake CH_4 emissions (Sepulveda-Jauregui et al., 2015; Walter et al., 2006).

Additionally, lakes are likely higher emitters during other times of the year. Some northern lakes have been observed to emit up to half of their annual C emissions during spring melt, when CO_2 and CH_4 that were trapped in the lake ice over the winter are released (Karlsson et al., 2013; Lundin et al., 2013). This means that the relative contribution of C emissions from ponds, lakes, and fluvial systems to regional C budgets is likely to be different in other seasons. For example, C emissions from lakes in western Siberia were observed to be twofold greater in spring, although this seasonal effect was not seen in fluvial emission rates (Serikova et al., 2018, 2019).

In our study area, small fluvial systems accounted for 20% of inland water C emissions (97% of which was CO_2-C), despite only covering 2% of the study area. This is in line with estimates on a global scale, indicating that fluvial systems account for more than 85% of inland water CO_2 emissions, despite only covering 17% of total inland water surface area (Raymond et al., 2013). It is also in agreement with estimates on regional scales, where small streams contributed 86% of the total fluvial CO_2 emissions in a 1,871 km^2 sub-watershed in northeast Siberia (Denfeld et al., 2013), and water tracks accounted for 53%–85% of total CH_4 emissions in a high Arctic catchment in Alaska (Harms et al., 2020). Additionally, we did not measure diurnal fluctuations, which have been shown to be significant in temperate regions, 27% higher than those estimates solely from diurnal concentrations (Gómez-Gener et al., 2021), but it is unknown whether inland water diurnal fluctuations are important in Arctic lowland tundra fluvial systems.

Certain relationships in inland water emission observations are present in several studies, indicating patterns that hold true at multiple scales throughout different northern high-latitude regions. One of these is the dominance of CO_2-C to total inland water C emissions compared to CH_4-C. CO_2-C contributed 97% of C emissions in our study compared to 3% CH_4-C. Similarly, in western Siberia, 90% of C emissions from small lakes were in the form of CO_2-C (Repo et al., 2007), as were 98% of C emissions from fluvial systems in western Siberia (Serikova et al., 2018), and in northern Sweden, CO_2-C emissions accounted for 98% of C emissions from streams and lakes (Lundin et al., 2013).

We estimate that inland waters offset the landscape C sink by 9%, with an associated estimated uncertainty of ±18%. When considering the conservative nature of our estimates, we do propose that inland waters are significant components of the carbon cycle in Arctic tundra lowlands. Specifically, our study indicates that small inland waters (ponds and low-order fluvial systems) are high CO_2 and CH_4 emitters in these landscapes. Despite being small in surface area, ponds can be highly abundant (Downing, 2010), and low-order fluvial systems account for the majority of stream length in many landscapes (Downing, 2012), and both systems are closely tied to the soil and riparian-wetland C release. Multiyear, spatially extensive sampling campaigns, combined with higher-resolution surface area data (Muster et al., 2017), will allow for more certain quantification of inland water contributions to regional C budgets.

4.2. Do N_2O Emissions Matter in This Arctic Tundra Landscape?

Our observed N_2O concentrations are comparable to values of inland waters in Québec, Canada; to our knowledge, the only other study with N_2O emission rates from inland waters in permafrost regions (Soued

et al., 2016). Our sampled inland water systems were undersaturated in N_2O relative to the atmosphere during the "normal" year. However, in the "wet" year, N_2O concentrations were higher, resulting in all inland water systems, besides ponds, being oversaturated with respect to the atmosphere. Interestingly, the "wet" year had a higher effect on N_2O concentrations compared to CO_2 and CH_4. Higher N_2O concentrations in 2017 were potentially due to the deeper snow cover and delayed snowmelt allowing for increased *N* mineralization in winter, resulting in higher *N* availability in summer. Increased N_2O fluxes in the Arctic soils due to deeper snow cover have been observed in snow fence experiments (Mörsdorf et al., 2020; Xu et al., 2023) and along a natural snowmelt gradient (Kolstad et al., 2021). The delayed snowmelt resulting in a wet landscape could explain the higher N_2O concentrations, as soil moisture (and oxygen availability) exhibit a large control on tundra N_2O production (Voigt et al., 2020). While we acknowledge that nitrogen availability and transformations (e.g., nitrification, denitrification) are important controls on N_2O production, this study does not include process-level measurements of inorganic nitrogen species (NO_3^- or NH_4^+). To our knowledge, such data are not available for this specific region. Our interpretations are therefore constrained to observed patterns in N_2O concentrations and hydrological context, rather than specific nitrogen cycling pathways. Contrary to our findings, N_2O undersaturation was observed in a year with higher-than-average summer rainfall in comparison to oversaturation during an average precipitation year in water tracks in Alaska (Harms et al., 2020). While this could indicate different effects on biogeochemical cycles due to different types of precipitation intensification, it could also be due to temperature effects or regional differences in topography, soil, and vegetation and the type of inland water sampled. The generally low N_2O emissions relative to CO_2 and CH_4 mean that variability in N_2O estimates is unlikely to significantly alter the overall contribution of N_2O emissions both in terms of inland water emissions and inland water emissions integrated with the landscape GHG exchange.

4.3. The Impact of Flooding

The floodwaters in the study area were estimated to cover 10% of the landscape and resulted in a 37% increase in inland water C emissions compared to the nonflood summer scenario. Floodwater contributions to total inland water C emissions were second only to ponds (40%) (Figure 7). We defined the floodwater separately from fluvial systems to isolate the effect of the flooding, although in reality, they are a single connected system. Our results show that when tundra becomes flooded, the landscape C sink is further offset because tundra that was previously acting as a C sink became a C source (i.e., behaves as an inland water system rather than primarily taking up carbon into plant biomass). Arctic tundra lowlands can readily be flooded, for example, during the spring snowmelt (Zakharova et al., 2009). In western Siberia, an estimated 30 days of flooding increased total inland water C emissions by ∼11%, supporting our findings (Karlsson et al., 2021). Climate change could further increase the magnitude and duration of flooding in tundra lowlands by changing precipitation patterns and altering local geomorphology as a result of permafrost thaw (Callaghan et al., 2011; Liljedahl et al., 2016). Precipitation, dominated by winter snowfall, has been predicted to increase for at least the next 40 years (Wang et al., 2023). In 2017, summer water levels in the Indigirka River, of which the Berelekh is a tributary, were the highest in 48 years of records, corresponding to an approximate 49-year return period (Tei et al., 2020). How long a landscape remains flooded will be crucial in determining to what degree flooding offsets the landscape C sink. The considerable influence of flooding on landscape C exchange with the atmosphere, offsetting the landscape C sink by an additional 4%, as observed in this study, indicates that the effects of flooding on regional Arctic C budgets could be considerable.

5. Conclusions

Emissions from small inland water systems such as ponds and low-order fluvial systems contributed disproportionately to landscape C exchange, relative to their small surface areas. Thus, our results indicate that such small inland water systems should be further investigated and included in upscaling exercises to accurately determine inland water C emissions in Arctic lowland tundra landscapes. Reliable data on surface area coverages of all inland water systems, coupled with direct measurements of dissolved CO_2 and CH_4 gas concentrations and emission rates in different Arctic regions, would allow for a better assessment of the overall importance of inland water C emissions to landscape C exchange across a range of scales. These improvements would facilitate more accurate estimation of Arctic C budgets and quantification of the permafrost carbon feedback.

Inclusion of N_2O emissions in the total radiative forcing estimates of inland water GHG emissions showed that despite the high warming potential of N_2O, its contribution to the net warming effect of total landscape GHG

exchange is negligible in our study area. This is in line with a general downward reevaluation of N_2O emissions from inland waters compared to the earlier studies (Hu et al., 2016; Lauerwald et al., 2019). However, very few direct observations of inland water N_2O emissions exist in the Arctic, and a better understanding of inland water N_2O concentration dynamics in high-latitude landscapes could enable predictions of not only how N_2O dynamics but also terrestrial and aquatic biogeochemical cycles could change under a warming climate.

Flooding caused a substantial additional offset to the landscape C sink capacity in our study area. This highlights the need for long-term and simultaneous monitoring of CO_2 and CH_4 emissions during flood events in the Arctic lowland tundra landscapes to gain a better understanding of their dynamics and possible feedback effects on future climate.

With continued Arctic warming, permafrost will continue to thaw and, as a result, alter tundra hydrology and carbon supply to inland water systems. It is therefore increasingly important to understand inland water carbon dynamics and to accurately determine their GHG emissions in the context of lowland tundra landscapes. Especially because the amount of carbon that is cycled through inland waters shows that they are a potentially important component of regional carbon cycles.

Data Availability Statement

The data used in this study are available at PANGAEA via https://doi.pangea.de/10.1594/PANGAEA.939906. The code written for this study is available on Zenodo: Melanie Martyn Rosco (2024). Upscaling [Code]. Zenodo. DOI: 10.5281/zenodo.14512643.

Acknowledgments
This work was carried out under the program of the Netherlands Earth System Science Centre (NESSC), financially supported by the Ministry of Education, Culture and Science (OCW). JFD received additional support from a UKRI Future Leaders Fellowships MR/V025082/1.

References

Abnizova, A., Siemens, J., Langer, M., & Boike, J. (2012). Small ponds with major impact: The relevance of ponds and lakes in permafrost landscapes to carbon dioxide emissions. *Global Biogeochemical Cycles*, *26*(2), GB2041. https://doi.org/10.1029/2011gb004237

Aufdenkampe, A. K., Mayorga, E., Raymond, P. A., Melack, J. M., Doney, S. C., Alin, S. R., et al. (2011). Riverine coupling of biogeochemical cycles between land, oceans, and atmosphere. *Frontiers in Ecology and the Environment*, *9*(1), 53–60. https://doi.org/10.1890/100014

Bates, D., Mächler, M., Bolker, B., & Walker, S. (2015). Fitting linear mixed-effects models using lme4. *Journal of Statistical Software*, *67*(1), 1–48. https://doi.org/10.18637/jss.v067.i01

Biskaborn, B. K., Smith, S. L., Noetzli, J., Matthes, H., Vieira, G., Streletskiy, D. A., et al. (2019). Permafrost is warming at a global scale. *Nature Communications*, *10*(1), 1–11. https://doi.org/10.1038/s41467-018-08240-4

Borges, A. V., Darchambeau, F., Lambert, T., Morana, C., Allen, G. H., Tambwe, E., et al. (2019). Variations in dissolved greenhouse gases (CO2, CH4, N2O) in the Congo River network overwhelmingly driven by fluvial-wetland connectivity. *Biogeosciences*, *16*(19), 3801–3834. https://doi.org/10.5194/bg-16-3801-2019

Borges, A. V., Darchambeau, F., Teodoru, C. R., Marwick, T. R., Tamooh, F., Geeraert, N., et al. (2015). Globally significant greenhouse-gas emissions from African inland waters. *Nature Geoscience*, *8*(8), 637–642. https://doi.org/10.1038/ngeo2486

Breiman, L. (2001). Random forests. *Machine Learning*, *45*(1), 5–32. https://doi.org/10.1023/A:1010933404324

Bulygina, O. N., Groisman, P. Y., Razuvaev, V. N., & Korshunova, N. N. (2011). Changes in snow cover characteristics over Northern Eurasia since 1966. *Environmental Research Letters*, *6*(4), 045204. https://doi.org/10.1088/1748-9326/6/4/045204

Callaghan, T. V., Johansson, M., Brown, R. D., Groisman, P. Y., Labba, N., Radionov, V., et al. (2011). The changing face of arctic snow cover: A synthesis of observed and projected changes. *Ambio*, *40*(SUPPL. 1), 17–31. https://doi.org/10.1007/s13280-011-0212-y

Cole, J. J., & Caraco, N. F. (1998). Atmospheric exchange of carbon dioxide in a low-wind oligotrophic lake measured by the addition of SF6. *Limnology & Oceanography*, *43*(4), 647–656. https://doi.org/10.4319/lo.1998.43.4.0647

Dean, J. F., Billett, M. F., Baxter, R., Dinsmore, K. J., Lessels, J. S., Street, L. E., et al. (2016). Biogeochemistry of "pristine" freshwater stream and lake systems in the western Canadian Arctic. *Biogeochemistry*, *130*(3), 191–213. https://doi.org/10.1007/s10533-016-0252-2

Dean, J. F., Meisel, O. H., Martyn Rosco, M., Marchesini, L. B., Garnett, M. H., Lenderink, H., et al. (2020). East Siberian Arctic inland waters emit mostly contemporary carbon. *Nature Communications*, *11*(1), 1–10. https://doi.org/10.1038/s41467-020-15511-6

Dean, J. F., Middelburg, J. J., Röckmann, T., Aerts, R., Blauw, L. G., Egger, M., et al. (2018). Methane feedbacks to the global climate system in a warmer world. *Reviews of Geophysics*, *56*(1), 207–250. https://doi.org/10.1002/2017RG000559

Denfeld, B. A., Frey, K. E., Sobczak, W. V., Mann, P. J., & Holmes, R. M. (2013). Summer CO2 evasion from streams and rivers in the Kolyma river basin, north-east Siberia. *Polar Research*, *32*(SUPPL.), 19704. https://doi.org/10.3402/polar.v32i0.19704

Denfeld, B. A., Wallin, M. B., Sahlée, E., Sobek, S., Kokic, J., Chmiel, H. E., & Weyhenmeyer, G. A. (2015). Temporal and spatial carbon dioxide concentration patterns in a small boreal lake in relation to ice-cover dynamics. *Boreal Environment Research*, *20*, 679–692.

Dentener, F. J. (2006). *Global maps of atmospheric nitrogen deposition, 1860, 1993, and 2050*. ORNL DAAC.

Dlugokencky, E. J., Lang, P. M., Masarie, K. A., Crotwell, A. M., & Crotwell, M. J. (2015). *Atmospheric carbon dioxide dry air mole fractions from the NOAA ESRL Carbon Cycle Cooperative Global Air Sampling Network, 1968—2014*. NOAA ESRL Global Monitoring Division.

Downing, J. (2010). Emerging global role of small lakes and ponds: Little things mean a lot. *Limnética*, *29*(1), 9–24. https://doi.org/10.23818/limn.29.02

Downing, J. (2012). Global abundance and size distribution of streams and rivers. *Inland Waters*, *2*(4), 229–236. https://doi.org/10.5268/IW-2.4.502

Drake, T. W., Raymond, P. A., & Spencer, R. G. M. (2018). Terrestrial carbon inputs to inland waters: A current synthesis of estimates and uncertainty: Terrestrial carbon inputs to inland waters. *Limnology and Oceanography Letters*, *3*(3), 132–142. https://doi.org/10.1002/lol2.10055

Efron, B. (1987). Better bootstrap confidence intervals. *Journal of the American Statistical Association*, *82*(397), 171–185. https://doi.org/10.1080/01621459.1987.10478410

Elder, C. D., Xu, X., Walker, J., Schnell, J. L., Hinkel, K. M., Townsend-Small, A., et al. (2018). Greenhouse gas emissions from diverse Arctic Alaskan lakes are dominated by young carbon. *Nature Climate Change*, *8*(2), 166–171. https://doi.org/10.1038/s41558-017-0066-9

Emmerton, C. A., St. Louis, V. L., Lehnherr, I., Graydon, J. A., Kirk, J. L., & Rondeau, K. J. (2016). The importance of freshwater systems to the net atmospheric exchange ofcarbon dioxide and methane with a rapidly changing high Arctic watershed. *Biogeosciences*, *13*(20), 5849–5863. https://doi.org/10.5194/bg-13-5849-2016

Gómez-Gener, L., Rocher-Ros, G., Battin, T., Cohen, M. J., Dalmagro, H. J., Dinsmore, K. J., et al. (2021). Global carbon dioxide efflux from rivers enhanced by high nocturnal emissions. *Nature Geoscience*, *14*(5), 289–294. Article 5. https://doi.org/10.1038/s41561-021-00722-3

Grosse, G., Jones, B., & Arp, C. (2013). Thermokarst lakes, drainage, and drained basins. In *Treatise on Geomorphology* (Vol. 8, pp. 325–353). Elsevier Ltd. https://doi.org/10.1016/B978-0-12-374739-6.00216-5

Grosse, G., Romanovsky, V. E., Walter, K. M., Morgenstern, A., Lantuit, H., & Zimov, S. (2008). Thermokarst lakes: High resolution distribution and temporal changes at three yedoma sites in Siberia. In *Proceedings from the Ninth International Conference on Permafrost* (pp. 551–556).

Harden, J. W., Koven, C. D., Ping, C. L., Hugelius, G., David McGuire, A., Camill, P., et al. (2012). Field information links permafrost carbon to physical vulnerabilities of thawing. *Geophysical Research Letters*, *39*(15), 1–6. https://doi.org/10.1029/2012GL051958

Harms, T. K., Rocher-Ros, G., & Godsey, S. E. (2020). Emission of greenhouse gases from water tracks draining arctic hillslopes. *Journal of Geophysical Research: Biogeosciences*, *125*(12), e2020JG005889. https://doi.org/10.1029/2020JG005889

Hensgens, G., Laudon, H., Johnson, M. S., & Berggren, M. (2021). The undetected loss of aged carbon from boreal mineral soils. *Scientific Reports*, *11*(1), 1–10. https://doi.org/10.1038/s41598-021-85506-w

Hersbach, H., Bell, B., Berrisford, P., Hirahara, S., Horányi, A., Muñoz-Sabater, J., et al. (2020). The ERA5 global reanalysis. *Quarterly Journal of the Royal Meteorological Society*, *146*(730), 1999–2049. https://doi.org/10.1002/qj.3803

Holgerson, M. A. (2015). Drivers of carbon dioxide and methane supersaturation in small, temporary ponds. *Biogeochemistry*, *124*(1–3), 305–318. https://doi.org/10.1007/s10533-015-0099-y

Holgerson, M. A., & Raymond, P. A. (2016). Large contribution to inland water CO2 and CH4 emissions from very small ponds. *Nature Geoscience*, *9*(3), 222–226. https://doi.org/10.1038/ngeo2654

Holgerson, M. A., Farr, E. R., & Raymond, P. A. (2017). Gas transfer velocities in small forested ponds: Gas exchange in small ponds. *Journal of Geophysical Research: Biogeosciences*, *122*(5), 1011–1021. https://doi.org/10.1002/2016JG003734

Hu, M., Chen, D., & Dahlgren, R. A. (2016). Modeling nitrous oxide emission from rivers: A global assessment. *Global Change Biology*, *22*(11), 3566–3582. https://doi.org/10.1111/gcb.13351

Hugelius, G., Strauss, J., Zubrzycki, S., Harden, J. W., Schuur, E. A. G., Ping, C. L., et al. (2014). Estimated stocks of circumpolar permafrost carbon with quantified uncertainty ranges and identified data gaps. *Biogeosciences*, *11*(23), 6573–6593. https://doi.org/10.5194/bg-11-6573-2014

Iwahana, G., Takano, S., Petrov, R. E., Tei, S., Shingubara, R., Maximov, T. C., et al. (2014). Geocryological characteristics of the upper permafrost in a tundra-forest transition of the Indigirka River Valley, Russia. *Polar Science*, *8*(2), 96–113. https://doi.org/10.1016/j.polar.2014.01.005

Jähne, B., Heinz, G., & Dietrich, W. (1987). Measurement of the diffusion coefficients of sparingly soluble gases in water. *Journal of Geophysical Research*, *92*(C10), 10767–10776. https://doi.org/10.1029/JC092iC10p10767

Jonasson, S., Michelsen, A., & Schmidt, I. K. (1999). Coupling of nutrient cycling and carbon dynamics in the Arctic, integration of soil microbial and plant processes. *Applied Soil Ecology*, *11*(2–3), 135–146. https://doi.org/10.1016/s0929-1393(98)00145-0

Jones, B. M., & Arp, C. D. (2015). Observing a catastrophic thermokarst lake drainage in northern Alaska. *Permafrost and Periglacial Processes*, *26*(2), 119–128. https://doi.org/10.1002/ppp.1842

Karlsson, J., Giesler, R., Persson, J., & Lundin, E. (2013). High emission of carbon dioxide and methane during ice thaw in high latitude lakes. *Geophysical Research Letters*, *40*(6), 1123–1127. https://doi.org/10.1002/grl.50152

Karlsson, J., Serikova, S., Vorobyev, S. N., Rocher-Ros, G., Denfeld, B., & Pokrovsky, O. S. (2021). Carbon emission from Western Siberian inland waters. *Nature Communications*, *12*(1), 1–8. https://doi.org/10.1038/s41467-021-21054-1

Kling, G. W., Kipphut, G. W., & Miller, M. C. (1991). Arctic lakes and streams as gas conduits to the atmosphere: Implications for tundra carbon budgets. *Science*, *251*(4991), 298–301. https://doi.org/10.1126/science.251.4991.298

Knoblauch, C., Spott, O., Evgrafova, S., Kutzbach, L., & Pfeiffer, E.-M. (2015). Regulation of methane production, oxidation, and emission by vascular plants and bryophytes in ponds of the northeast Siberian polygonal tundra. *Journal of Geophysical Research: Biogeosciences*, *120*(12), 2525–2541. https://doi.org/10.1002/2015JG003053

Kolstad, E., Michelsen, A., & Ambus, P. L. (2021). Nitrous oxide surface fluxes in a low Arctic heath: Effects of experimental warming along a natural snowmelt gradient. *Soil Biology and Biochemistry*, *160*, 108346. https://doi.org/10.1016/j.soilbio.2021.108346

Kortelainen, P., Larmola, T., Rantakari, M., Juutinen, S., Alm, J., & Martikainen, P. J. (2020). Lakes as nitrous oxide sources in the boreal landscape. *Global Change Biology*, *26*(3), 1432–1445. https://doi.org/10.1111/gcb.14928

Kortelainen, P., Rantakari, M., Huttunen, J. T., Mattsson, T., Alm, J., Juutinen, S., et al. (2006). Sediment respiration and lake trophic state are important predictors of large CO2 evasion from small boreal lakes. *Global Change Biology*, *12*(8), 1554–1567. https://doi.org/10.1111/j.1365-2486.2006.01167.x

Krickov, I. V., Serikova, S., Pokrovsky, O. S., Vorobyev, S. N., Lim, A. G., Siewert, M. B., & Karlsson, J. (2021). Sizable carbon emission from the floodplain of Ob River. *Ecological Indicators*, *131*, 108164. https://doi.org/10.1016/j.ecolind.2021.108164

Kuhn, M., Lundin, E. J., Giesler, R., Johansson, M., & Karlsson, J. (2018). Emissions from thaw ponds largely offset the carbon sink of northern permafrost wetlands. *Scientific Reports*, *8*(1), 9535. https://doi.org/10.1038/s41598-018-27770-x

Kuhn, M., Thompson, L. M., Winder, J. C., Braga, L. P. P., Tanentzap, A. J., Bastviken, D., & Olefeldt, D. (2021). Opposing effects of climate and permafrost thaw on CH_4 and CO_2 emissions from northern lakes. *AGU Advances*, *2*(4), e2021AV000515. https://doi.org/10.1029/2021AV000515

Lauerwald, R., Regnier, P., Figueiredo, V., Enrich-Prast, A., Bastviken, D., Lehner, B., et al. (2019). Natural lakes are a minor global source of N2O to the atmosphere. *Global Biogeochemical Cycles*, *33*(12), 1564–1581. https://doi.org/10.1029/2019GB006261

Liljedahl, A. K., Boike, J., Daanen, R. P., Fedorov, A. N., Frost, G. V., Grosse, G., et al. (2016). Pan-Arctic ice-wedge degradation in warming permafrost and its influence on tundra hydrology. *Nature Geoscience*, *9*(4), 312–318. https://doi.org/10.1038/ngeo2674

Linke, S., Lehner, B., Ouellet Dallaire, C., Ariwi, J., Grill, G., Anand, M., et al. (2019). Global hydro-environmental sub-basin and river reach characteristics at high spatial resolution. *Scientific Data*, *6*(1), 283. https://doi.org/10.1038/s41597-019-0300-6

Liu, S., Kuhn, C., Amatulli, G., Aho, K., Butman, D. E., Allen, G. H., et al. (2022). The importance of hydrology in routing terrestrial carbon to the atmosphere via global streams and rivers. *Proceedings of the National Academy of Sciences*, *119*(11), e2106322119. https://doi.org/10.1073/pnas.2106322119

Lundin, E. J., Giesler, R., Persson, A., Thompson, M. S., & Karlsson, J. (2013). Integrating carbon emissions from lakes and streams in a subarctic catchment. *Journal of Geophysical Research: Biogeosciences*, *118*(3), 1200–1207. https://doi.org/10.1002/jgrg.20092

Martikainen, P. J., Nykänen, H., Crill, P., & Silvola, J. (1993). Effect of a lowered water table on nitrous oxide fluxes from northern peatlands. *Nature*, *366*(6450), 51–53. https://doi.org/10.1038/366051a0

Meredith, M., Sommerkorn, M., Cassotta, S., Derksen, C., Ekaykin, A., Hollowed, A., et al. (2019). Polar regions. In H.-O. Pörtner, et al. (Eds.), *IPCC Special Report on the Ocean and Cryosphere in a Changing Climate*. https://doi.org/10.1016/S1366-7017(01)00066-6

Morozumi, T., Shingubara, R., Murase, J., Nagai, S., Kobayashi, H., Takano, S., et al. (2019). Usability of water surface reflectance for the determination of riverine dissolved methane during extreme flooding in northeastern Siberia. *Polar Science*, *21*(June 2018), 186–194. https://doi.org/10.1016/j.polar.2019.01.005

Mörsdorf, M. A., Baggesen, N. S., Yoccoz, N. G., Michelsen, A., Elberling, B., Ambus, P. L., & Cooper, E. J. (2020). Deepened winter snow significantly influences the availability and forms of nitrogen taken up by plants in High Arctic tundra. *Soil Biology and Biochemistry*, *142*, 107654. https://doi.org/10.1016/j.soilbio.2019.107654

Muster, S., Langer, M., Heim, B., Westermann, S., & Boike, J. (2012). Subpixel heterogeneity of ice-wedge polygonal tundra: A multi-scale analysis of land cover and evapotranspiration in the Lena river Delta, Siberia. *Tellus B: Chemical and Physical Meteorology*, *64*(1), 17301. https://doi.org/10.3402/tellusb.v64i0.17301

Muster, S., Roth, K., Langer, M., Lange, S., Cresto Aleina, F., Bartsch, A., et al. (2017). PeRL: A circum-arctic permafrost region pond and lake database. *Earth System Science Data*, *9*(1), 317–348. https://doi.org/10.5194/essd-9-317-2017

Neubauer, S. C., & Megonigal, J. P. (2015). Moving beyond global warming potentials to quantify the climatic role of ecosystems. *Ecosystems*, *18*(6), 1000–1013. https://doi.org/10.1007/s10021-015-9879-4

Nitzbon, J., Westermann, S., Langer, M., Martin, L. C. P., Laboor, S., & Boike, J. (2020). Fast response of cold ice-rich permafrost in northeast Siberia to a warming climate. *Nature Communications*, *11*(1), 2201. https://doi.org/10.1038/s41467-020-15725-8

Papale, D., Reichstein, M., Canfora, E., Aubinet, M., Bernhofer, C., Longdoz, B., et al. (2006). Towards a more harmonized processing of eddy covariance CO_2 fluxes: Algorithms and uncertainty estimation. *Biogeosciences Discussions*, *3* (4), 961–992. Retrieved from https://bg.copernicus.org/preprints/3/961/2006/bgd-3-961-2006-print.pdf

Parmentier, F. J. W., Van Huissteden, J., Van Der Molen, M. K., Schaepman-Strub, G., Karsanaev, S. A., Maximov, T. C., & Dolman, A. J. (2011). Spatial and temporal dynamics in eddy covariance observations of methane fluxes at a tundra site in northeastern Siberia. *Journal of Geophysical Research*, *116*(3), 1–14. https://doi.org/10.1029/2010JG001637

Pedregosa, F., Varoquaux, G., Gramfort, A., Michel, V., Thirion, B., Grisel, O., et al. (2011). Scikit-learn: Machine learning in Python. *Journal of Machine Learning Research*, *12*, 2825–2830.

R Core Team. (2019). *R: A Language and Environment for Statistical Computing*. R Foundation for Statistical Computing. Retrieved from https://www.R-project.org/

Rantakari, M., & Kortelainen, P. (2005). Interannual variation and climatic regulation of the CO2 emission from large boreal lakes. *Global Change Biology*, *11*(8), 1368–1380. https://doi.org/10.1111/j.1365-2486.2005.00982.x

Raymond, P. A., Hartmann, J., Lauerwald, R., Sobek, S., McDonald, C., Hoover, M., et al. (2013). Global carbon dioxide emissions from inland waters. *Nature*, *503*(7476), 355–359. https://doi.org/10.1038/nature12760

Raymond, P. A., McClelland, J. W., Holmes, R. M., Zhulidov, A. V., Mull, K., Peterson, B. J., et al. (2007). Flux and age of dissolved organic carbon exported to the arctic ocean: A carbon isotopic study of the five largest arctic rivers. *Global Biogeochemical Cycles*, *21*(4), 1–9. https://doi.org/10.1029/2007GB002934

Raymond, P. A., Zappa, C. J., Butman, D., Bott, T. L., Potter, J., Mulholland, P., et al. (2012). Scaling the gas transfer velocity and hydraulic geometry in streams and small rivers: Gas transfer velocity and hydraulic geometry. *Limnology and Oceanography: Fluids and Environments*, *2*(1), 41–53. https://doi.org/10.1215/21573689-1597669

Repo, M. E., Huttunen, J. T., Naumov, A. V., Chichulin, A. V., Lapshina, E. D., Bleuten, W., & Martikainen, P. J. (2007). Release of CO2 and CH4 from small wetland lakes in western Siberia. *Tellus Series B Chemical and Physical Meteorology*, *59*(5), 788–796. https://doi.org/10.1111/j.1600-0889.2007.00301.x

Rocher-Ros, G., Giesler, R., Lundin, E., Salimi, S., Jonsson, A., & Karlsson, J. (2017). Large lakes dominate CO_2 evasion from lakes in an arctic catchment. *Geophysical Research Letters*, *44*(24), 12254–12261. https://doi.org/10.1002/2017GL076146

Rodionow, A., Flessa, H., Kazansky, O., & Guggenberger, G. (2006). Organic matter composition and potential trace gas production of permafrost soils in the forest tundra in northern Siberia. *Geoderma*, *135*, 49–62. https://doi.org/10.1016/j.geoderma.2005.10.008

Rosentreter, J. A., Borges, A. V., Deemer, B. R., Holgerson, M. A., Liu, S., Song, C., et al. (2021). Half of global methane emissions come from highly variable aquatic ecosystem sources. *Nature Geoscience*, *14*(4), 225–230. https://doi.org/10.1038/s41561-021-00715-2

Rusydi, A. F. (2018). Correlation between conductivity and total dissolved solid in various type of water: A review. *IOP Conference Series: Earth and Environmental Science*, *118*, 012019. https://doi.org/10.1088/1755-1315/118/1/012019

Schuur, E. A. G. G., McGuire, A. D., Schädel, C., Grosse, G., Harden, J. W., Hayes, D. J., et al. (2015). Climate change and the permafrost carbon feedback. *Nature*, *520*(7546), 171–179. https://doi.org/10.1038/nature14338

Schwab, M. S., Hilton, R. G., Raymond, P. A., Haghipour, N., Amos, E., Tank, S. E., et al. (2020). An Abrupt aging of dissolved organic carbon in large arctic rivers. *Geophysical Research Letters*, *47*(23), e2020GL088823. https://doi.org/10.1029/2020GL088823

Sepulveda-Jauregui, A., Walter Anthony, K. M., Martinez-Cruz, K., Greene, S., & Thalasso, F. (2015). Methane and carbon dioxide emissions from 40 lakes along a north–south latitudinal transect in Alaska. *Biogeosciences*, *12*(11), 3197–3223. https://doi.org/10.5194/bg-12-3197-2015

Serikova, S., Pokrovsky, O. S., Ala-Aho, P., Kazantsev, V., Kirpotin, S. N., Kopysov, S. G., et al. (2018). High riverine CO2 emissions at the permafrost boundary of Western Siberia. *Nature Geoscience*, *11*(11), 825–829. https://doi.org/10.1038/s41561-018-0218-1

Serikova, S., Pokrovsky, O. S., Laudon, H., Krickov, I. V., Lim, A. G., Manasypov, R. M., & Karlsson, J. (2019). High carbon emissions from thermokarst lakes of Western Siberia. *Nature Communications*, *10*(1), 1–7. https://doi.org/10.1038/s41467-019-09592-1

Shahgedanova, M. (Ed.). (2003). *The physical geography of northern Eurasia* (Vol. 3). Oxford University Press.

Soued, C., Del Giorgio, P. A., & Maranger, R. (2016). Nitrous oxide sinks and emissions in boreal aquatic networks in Quebec. *Nature Geoscience*, *9*(2), 116–120. https://doi.org/10.1038/ngeo2611

Tei, S., Morozumi, T., Nagai, S., Takano, S., Sugimoto, A., Shingubara, R., et al. (2020). An extreme flood caused by a heavy snowfall over the Indigirka River basin in Northeastern Siberia. *Hydrological Processes*, *34*(3), 522–537. https://doi.org/10.1002/hyp.13601

Thackeray, C. W., Derksen, C., Fletcher, C. G., & Hall, A. (2019). Snow and climate: Feedbacks, drivers, and Indices of change. *Current Climate Change Reports*, *5*(4), 322–333. https://doi.org/10.1007/s40641-019-00143-w

Trouet, V., & Oldenborgh, G. J. V. (2013). KNMI climate explorer: A web-based research tool for high-resolution paleoclimatology. *Tree-Ring Research*, *69*(1), 3–13. https://doi.org/10.3959/1536-1098-69.1.3

van Huissteden, J., Teshebaeva, K., Cheung, Y., Magnússon, R. Í., Noorbergen, H., Karsanaev, S. V., et al. (2021). Geomorphology and InSAR-tracked surface displacements in an ice-rich yedoma landscape. *Frontiers in Earth Science*, *9*. https://doi.org/10.3389/feart.2021.680565

Van Rossum, G., & Drake, F. L. (2009). Python 3 reference manual. *CreateSpace*.

Voigt, C., Marushchak, M. E., Abbott, B. W., Biasi, C., Elberling, B., Siciliano, S. D., et al. (2020). Nitrous oxide emissions from permafrost-affected soils. *Nature Reviews Earth and Environment*, *1*(8), 420–434. https://doi.org/10.1038/s43017-020-0063-9

Voigt, C., Marushchak, M. E., Lamprecht, R. E., Jackowicz-Korczyński, M., Lindgren, A., Mastepanov, M., et al. (2017). Increased nitrous oxide emissions from Arctic peatlands after permafrost thaw. *Proceedings of the National Academy of Sciences of the United States of America*, *114*(24), 6238–6243. https://doi.org/10.1073/pnas.1702902114

Vonk, J. E., Tank, S. E., Bowden, W. B., Laurion, I., Vincent, W. F., Alekseychik, P., et al. (2015). Reviews and syntheses: Effects of permafrost thaw on Arctic aquatic ecosystems. *Biogeosciences*, *12*(23), 7129–7167. https://doi.org/10.5194/bg-12-7129-2015

Vorobyev, S. N., Karlsson, J., Kolesnichenko, Y. Y., Korets, M. A., & Pokrovsky, O. S. (2021). Fluvial carbon dioxide emission from the Lena River basin during the spring flood. *Biogeosciences*, *18*(17), 4919–4936. https://doi.org/10.5194/bg-18-4919-2021

Walker, D. A., Reynolds, M. K., Daniëls, F. J. A., Einarsson, E., Elvebakk, A., Gould, W. A., et al. (2005). The Circumpolar Arctic vegetation map. *Journal of Vegetation Science*, *16*(3), 267–282. https://doi.org/10.1111/j.1654-1103.2005.tb02365.x

Walter, K. M., Zimov, S. A., Chanton, J. P., Verbyla, D., & Chapin, F. S. (2006). Methane bubbling from Siberian thaw lakes as a positive feedback to climate warming. *Nature*, *443*(7107), 71–75. https://doi.org/10.1038/nature05040

Wang, Z., Wu, R., Chen, Z., Huang, G., & Yang, X. (2023). Reasons for east Siberia winter snow water equivalent increase in the recent decades. *Remote Sensing*, *15*(1), 134. Article 1. https://doi.org/10.3390/rs15010134

Wanninkhof, R. (2014). Relationship between wind speed and gas exchange over the ocean revisited. *Limnology and Oceanography: Methods*, *12*(6), 351–362. https://doi.org/10.4319/lom.2014.12.351

Webb, J. R., Santos, I. R., Maher, D. T., & Finlay, K. (2019). The importance of aquatic carbon fluxes in net ecosystem carbon budgets: A catchment-scale review. *Ecosystems*, *22*(3), 508–527. https://doi.org/10.1007/s10021-018-0284-7

Weiss, R. F. (1974). Carbon dioxide in water and seawater: The solubility of a non-ideal gas. *Marine Chemistry*, *2*(3), 203–215. https://doi.org/10.1016/0304-4203(74)90015-2

Weiss, R. F., & Price, B. A. (1980). Nitrous oxide solubility in water and seawater. *Marine Chemistry*, *8*(4), 347–359. https://doi.org/10.1016/0304-4203(80)90024-9

Wik, M., Varner, R. K., Anthony, K. W., MacIntyre, S., & Bastviken, D. (2016). Climate-sensitive northern lakes and ponds are critical components of methane release. *Nature Geoscience*, *9*(2), 99–105. https://doi.org/10.1038/ngeo2578

Xu, W., Frendrup, L. L., Michelsen, A., Elberling, B., & Ambus, P. L. (2023). Deepened snow in combination with summer warming increases growing season nitrous oxide emissions in dry tundra, but not in wet tundra. *Soil Biology and Biochemistry*, *180*, 109013. https://doi.org/10.1016/j.soilbio.2023.109013

Yamamoto, S., Alcauskas, J. B., & Crozier, T. E. (1976). Solubility of methane in distilled water and seawater. *Journal of Chemical and Engineering Data*, *21*(1), 78–80. https://doi.org/10.1021/je60068a029

Yvon-Durocher, G., Allen, A. P., Bastviken, D., Conrad, R., Gudasz, C., St-Pierre, A., et al. (2014). Methane fluxes show consistent temperature dependence across microbial to ecosystem scales. *Nature*, *507*(7493), 488–491. Article 7493. https://doi.org/10.1038/nature13164

Zakharova, E. A., Kouraev, A. V., Kolmakova, M. V., Mognard, N. M., Zemtsov, V. A., & Kirpotin, S. N. (2009). The modern hydrological regime of the Northern part of Western Siberia from in situ and satellite observations. *International Journal of Environmental Studies*, *66*(4), 447–463. https://doi.org/10.1080/00207230902823578

Zuur, A. F., Leno, E. N., Walker, N., Saveliev, A. A., & Smith, G. M. (2009). *Mixed Effects Models and Extensions in Ecology with R* (1st ed.). Springer.